

RESEARCH ARTICLE

10.1002/2016JD025463

Key Points:

- A 106 year long record of Baiu frontal activity from tree ring isotope data
- Interdecadal variability of Baiu activity back through the twentieth century
- Interdecadal modulation of the impact of teleconnections on Baiu activity

Correspondence to:

N. Kurita,
kurita.naoyuki@e.mbox.nagoya-u.ac.jp

Citation:

Kurita, N., T. Nakatsuka, K. Ohnishi, T. Mitsutani, and T. Kumagai (2016), Analysis of the interdecadal variability of summer precipitation in central Japan using a reconstructed 106 year long oxygen isotope record from tree ring cellulose, *J. Geophys. Res. Atmos.*, 121, 12,089–12,107, doi:10.1002/2016JD025463.

Received 10 JUN 2016

Accepted 30 SEP 2016

Accepted article online 5 OCT 2016

Published online 28 OCT 2016

Analysis of the interdecadal variability of summer precipitation in central Japan using a reconstructed 106 year long oxygen isotope record from tree ring cellulose

Naoyuki Kurita¹, Takeshi Nakatsuka^{2,3}, Keiko Ohnishi⁴, Takumi Mitsutani⁵, and Tomo'omi Kumagai¹

¹Institute for Space-Earth Environmental Research, Nagoya University, Nagoya, Japan, ²Graduate School of Environmental Studies, Nagoya University, Nagoya, Japan, ³Research Institute for Humanity and Nature, Motoyama, Kyoto, Japan, ⁴Institute of Low Temperature Science, Hokkaido University, Sapporo, Japan, ⁵Nara National Research Institute for Cultural Properties, Nara, Japan

Abstract We present a unique proxy for reconstructing the interannual variability of summer precipitation associated with the quasi-stationary front (Baiu front) in central Japan. The rainfall from the Baiu front has a relatively lower oxygen isotopic composition than other types of nonfrontal precipitation. The variability in the oxygen isotopes in summer rainfall is closely related to the Baiu frontal activity. In this study we used a mechanistic tree ring isotope model to reconstruct a 106 year long oxygen isotopic composition of precipitation during the early rainy season (June) based on the oxygen isotopic compositions of the annual rings of *Chamaecyparis obtusa* Endl trees from central Japan. The year-to-year variations of the isotopes over the most recent 25 years are associated with several teleconnection patterns that often lead to the Baiu precipitation anomalies in central Japan (such as the Pacific-Japan (PJ) pattern, Silk Road pattern, and wave train pattern along the polar jet). Yet none of these external forcing mechanisms apply further back in time. From the 1950s to 1980s, the interannual isotopic variability is predominantly related to local factors such as anomalous intensification/weakening of the Bonin High. Before the 1950s, the variability of the oxygen isotopic composition of precipitation is mainly associated with a wave train pattern along the polar jet. The isotopic variability is predominantly linked to the PJ pattern, while the PJ index is correlated with El Niño–Southern Oscillation. These findings suggest that the teleconnection patterns influencing Baiu precipitation variability vary according to interdecadal time scales during the twentieth century.

1. Introduction

The East Asian summer monsoon (EASM) is characterized by a northward migrating rainband referred to as “Meiyu” in China and “Baiu” in Japan [e.g., Yihui and Chan, 2005; Ninomiya et al., 1987]. This rainband appears in mid-May in the South China Sea and then migrates northward to the Yangtze River Valley and Japan from early June to mid-July. In mid-July, the rainband abruptly jumps to northern China and Korea, ending the rainy season. Owing to the interannual variability of the EASM, the activity and migration speed of the rainband vary widely year-by-year. Seasonality and changes in the rainfall amount affect the livelihoods of billions of people in East Asia, a region encompassing China, Japan, and Korea. For example, severe droughts struck the Yangtze River basin during years when the rainband arrived comparatively late or moved quickly northward [Gemmer et al., 2012]. In other years when the region received more precipitation during the rainy season, the basin was flooded. In Japan, where the rainy season lasts longer than usual, the record-cold summer of 1993 caused a serious failure of the rice harvest. A reliable interpretation of the impact of climate variability on the EASM is important for the sustainable development of billions of people.

The seasonal transition of the rainband corresponds well to the seasonal evolution of the westerly jet impinging on the Tibetan Plateau (TP) [Schiemann et al., 2009]. The Meiyu-Baiu rainband is formed along the downstream of the westerly jet, where the advection of warm air by westerlies induces an ascending motion that triggers convection to form the rainband [Sampe and Xie, 2010]. Changes in midtropospheric circulation patterns cause the summer precipitation to vary over East Asia [Kosaka et al., 2011]. Knowing this, we can reasonably deduce that the variability of the rainband on an interannual time scale is closely related to circulation anomalies associated with teleconnection patterns such as the El Niño–Southern Oscillation (ENSO)

[e.g., Tanaka, 1997], Silk Road pattern, wave train-like pattern along the summer Asian jet (40°N) over the Eurasian continent [e.g., Enomoto *et al.*, 2003], and the Pacific-Japan (PJ) pattern (the meridional dipole of anomalous circulation over the northwestern Pacific (NWP)) [e.g., Nitta, 1987]. Recent studies, however, raise questions as to whether these external forcing mechanisms will persist through all future time. Xie *et al.* [2010], for example, reported that El Niño exerts a more manifest influence on the EASM after wielding an insignificant influence from the 1950s up to the climate regime shift of the mid-1970s. Variability in the Meiyu-Baiu rainband has been examined using reanalysis data sets, but their data source limits the scope of their analysis to the latter half of the twentieth century. The available data sets cover too short a period to exhibit interdecadal modulation in the frequency and intensity of teleconnection patterns. To detect anthropogenically forced changes, our record must be extended back in time beyond the twentieth century [Stott *et al.*, 2010]. These require alternative approaches to examine the long-term variations of the rainband activity, including proxy data obtained from natural proxies.

This study reconstructs the past Baiu rainband activity in central Japan using annually resolved records of oxygen isotopic compositions in tree rings from coniferous trees. Trees are widely distributed and provide precisely dated records of climatic variables during the growing season (summer) beyond the period with available data sets for reliable reanalysis: in effect, the number of meteorological stations becomes comparable with that today (the latter half of the twentieth century). The oxygen isotopic composition of tree ring cellulose reflects both the oxygen isotopic concentration of the soil water taken up by the trees (source water) and the isotopic fractionations that occur within the trees, mainly through leaf water evaporative enrichment during transpiration and the physiological processes of cellulose synthesis (see Barbour [2007] for a detailed review). The process of isotopic exchange with source water during cellulose synthesis reduces the effect of evaporative enrichment on the tree ring isotope signal [e.g., Roden *et al.*, 2000]. Thus, the isotope signal of source water is a dominant determinant of the oxygen isotopic composition of tree ring cellulose [e.g., Edwards and Fritz, 1986; Saurer *et al.*, 1997a; Danis *et al.*, 2006; Brienen *et al.*, 2013]. The isotope signal of source water represents an integrated signal of soil water from multiple root zones. The soil water is recharged by precipitation during the summer rainy season. For coniferous trees with shallow root systems, the oxygen isotopic composition of source water may be more reflective of the oxygen isotopic composition of summer precipitation than that of groundwater [e.g., Anderson *et al.*, 2002; Miller *et al.*, 2006; Brienen *et al.*, 2012; Saurer *et al.*, 2015]. In central Japan, the isotopic variations in summer precipitation can be related to a meridional position of the Baiu rainband [Kurita *et al.*, 2013]. The Baiu rainband appears along the quasi-stationary front (Baiu front) between the warm moist air with enriched isotopic values from the subtropics and the dry cool air with depleted isotopic values to the north. The average isotopic value in summer will be lower (higher) than that of a normal year if the rainy season lasts longer (shorter) than usual.

In this study we reconstruct a 106 year long record of Baiu rainband activity in central Japan by examining the tree ring oxygen isotopes. We then apply the reconstructed record to examine whether the variability of Baiu rainband activity in response to changes in atmospheric circulation associated with teleconnection patterns persists through the twentieth century. The long-term record of Baiu rainband activity has the potential not only to discern the long-term trend and its multidecadal variability but also to assess the influences of anthropogenically forced changes. A mechanistic tree ring isotope model that can precisely predict variability in the oxygen isotopic composition of tree rings has already been established [e.g., Roden *et al.*, 2000; Barbour *et al.*, 2004; Barbour, 2007; Sternberg, 2008]. We therefore use this model to estimate a long-term record of the isotopic composition of source water and summer precipitation as an indicator of Baiu rainband activity.

2. Materials and Methods

2.1. Study Site

The tree ring sampling for this study was carried out in a temperate coniferous forest at Agematsu, in central Japan (33.75°N, 137.58°E, 1280 meters above sea level (masl)) (Figure 1). The mean annual temperature at the study site is around 10.1°C, with a minimum monthly mean of −2.2°C in January and a maximum monthly mean of 22.8°C in August. The mean annual precipitation is about 1680 mm. The rainfall is seasonal, with a pronounced dry winter season from December to February (<60 mm month^{−1}) and a Baiu rainy season delivering about 30% of the annual rainfall from early June to mid-July. The number of typhoons approaching the Japanese archipelago is much higher in boreal summer and late summer than in the rainy period.



Figure 1. Topographical map of central Japan showing the locations of the sampling site (Agematsu), meteorological stations (Iida and Nagiso), and isotope monitoring stations (Tokyo and Nagoya).

2.2. Tree Ring Isotope Data

Four wood disks of *Chamaecyparis obtusa* Endl (Japanese cypress) were collected in 2005 from an evergreen coniferous plantation on a northerly facing slope of the mountainous region at Agematsu. Coniferous trees in temperate regions are well suited for reconstructing the oxygen isotopic compositions of summer precipitation because of their shallow root systems [e.g., Anderson *et al.*, 2002; Miller *et al.*, 2006; Brienen *et al.*, 2012; Saurer *et al.*, 2015]. We therefore chose to reconstruct the oxygen isotopic compositions using *Ch. obtusa*, a common coniferous tree species that has long been cultivated in Japan by confirmed silvicultural methods [Tatman, 1989]. *Ch. obtusa* is a massive evergreen coniferous tree that can grow to a height up to 35 m and a trunk diameter of up to 1 m. *Ch. obtusa* grows under moderate temperature and soil moisture conditions. *Ch. obtusa* plantation forests are now widespread in central Japan, though native forests are nearly gone, existing only in remnant stands. Given the climate conditions in the central Japan region where *Ch. obtusa* is planted, we can expect somewhat homogeneous wood properties and a relative absence of physiological stresses. *Ch. obtusa* forms distinct annual tree rings that closely match the ages of the tree. The annual nature of the growth rings for our samples was proven by visually matching ring-width patterns against a master chronology developed by Mitsutani [1987a] and Mitsutani [1987b]. This result is also supported by a significant ($p < 0.001$) intercorrelation between individual $\delta^{18}\text{O}$ time series from four samples (see below).

The oxygen isotope data used in this study were measured at two different laboratories: the Institute of Low Temperature Science (ILTS) at Hokkaido University and the Research Institute for Humanity and Nature (RIHN).

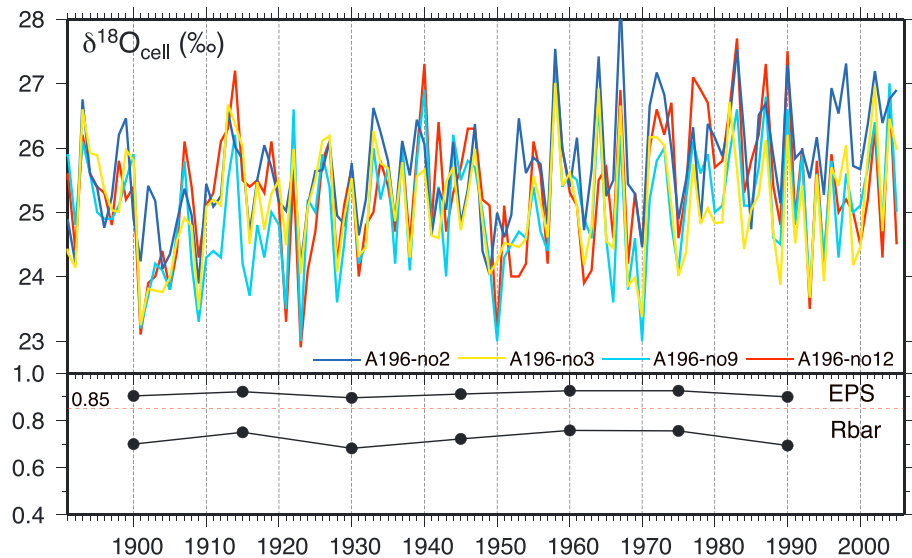


Figure 2. Time series of individual tree ring $\delta^{18}\text{O}$ obtained from the four samples of *Ch. obtusa* at the Agematus site (color lines) and running EPS and Rbar computed over 30 year windows, lagged by 15 years.

The oxygen isotope analysis for two of the disks (245 and 276 years old) was performed at ITLS using a method developed by, e.g., Loader *et al.* [1997]. All of the annual rings were cut out carefully with a utility knife and sliced into thin slivers with a razor blade. Samples of α -cellulose were extracted from each sliver using a method described by Harada *et al.* [2014]. The oxygen isotopic composition of the α -cellulose samples extracted from the rings (120–200 μg) were determined by loading the samples into a silver capsule and transferring them into a High-Temperature Combustion Elemental Analyzer (TC/EA; Thermo Finnigan, Bremen, Germany) linked to a mass spectrometer (Delta plus XL; Thermo Fisher Scientific). Each sample was analyzed in duplicate to obtain more precise data. The oxygen isotopic composition of each tree ring was averaged and converted into a δ value with respect to the international standard Vienna standard mean ocean water (V-SMOW), an international standard: $\delta^{18}\text{O} = \frac{R}{R_{\text{VSMOW}} - 1}$, where R_{VSMOW} is R for VSMOW. The analytical precision of a laboratory working standard (Merck cellulose; Darmstadt, Germany) measurement was about 0.15‰ (1σ). The oxygen isotopic analyses for the other two wood disks (167 and 179 years old) were conducted at RIHN, using a “cross-section” method for α -cellulose extraction [Kagawa *et al.*, 2015]. This method extracts α -cellulose not from individual rings but directly from a 1 mm thick tree ring plate. The tree ring cellulose samples were then cut from the α -cellulose plate, weighted, and wrapped into silver foil. Kagawa *et al.* [2015] found no significant difference between the $\delta^{18}\text{O}$ values determined by the cross-section method and those determined by the conventional method. This method has already been applied to several species [e.g., Xu *et al.*, 2011, 2013; Sano *et al.*, 2013; Xu *et al.*, 2016]. The oxygen isotope ratios were measured using a continuous flow isotope ratio mass spectrometer (Delta V Advantage; Thermo Fisher Scientific) coupled with the TC/EA. The analytical uncertainties associated with repeated measurements of the working standard were $\pm 0.14\text{‰}$. The $\delta^{18}\text{O}$ values measured at ITLS and RIHN did not significantly differ, as both laboratories converted the oxygen isotope ratios to δ values with respect to the V-SMOW using the same working standard (Merck cellulose).

The oxygen isotopic compositions obtained from the four trees show high synchronization over the 100 years from 1885 to 2005, though distinct age-related biases (juvenile effects) [e.g., Treydte *et al.*, 2006] appear during their early growth stage before 1850 Common Era. As shown in Figure 2, a running correlation for the $\delta^{18}\text{O}$ chronology using a 30 year window with an overlap of 15 years exhibits a good intertree correlation (Rbar) among the four trees throughout the entire period (Rbar > 0.68). The running expressed population signal (EPS), a parameter calculated using Rbar and the number of samples [Wigley *et al.*, 1984], exceeded the threshold value of 0.85 (EPS > 0.90), testifying to the robustness of the $\delta^{18}\text{O}$ chronology based on the four *Ch. obtusa* trees. We thus used the arithmetic mean oxygen isotopic ratios of the four trees in all of the analyses (Figure 3a).

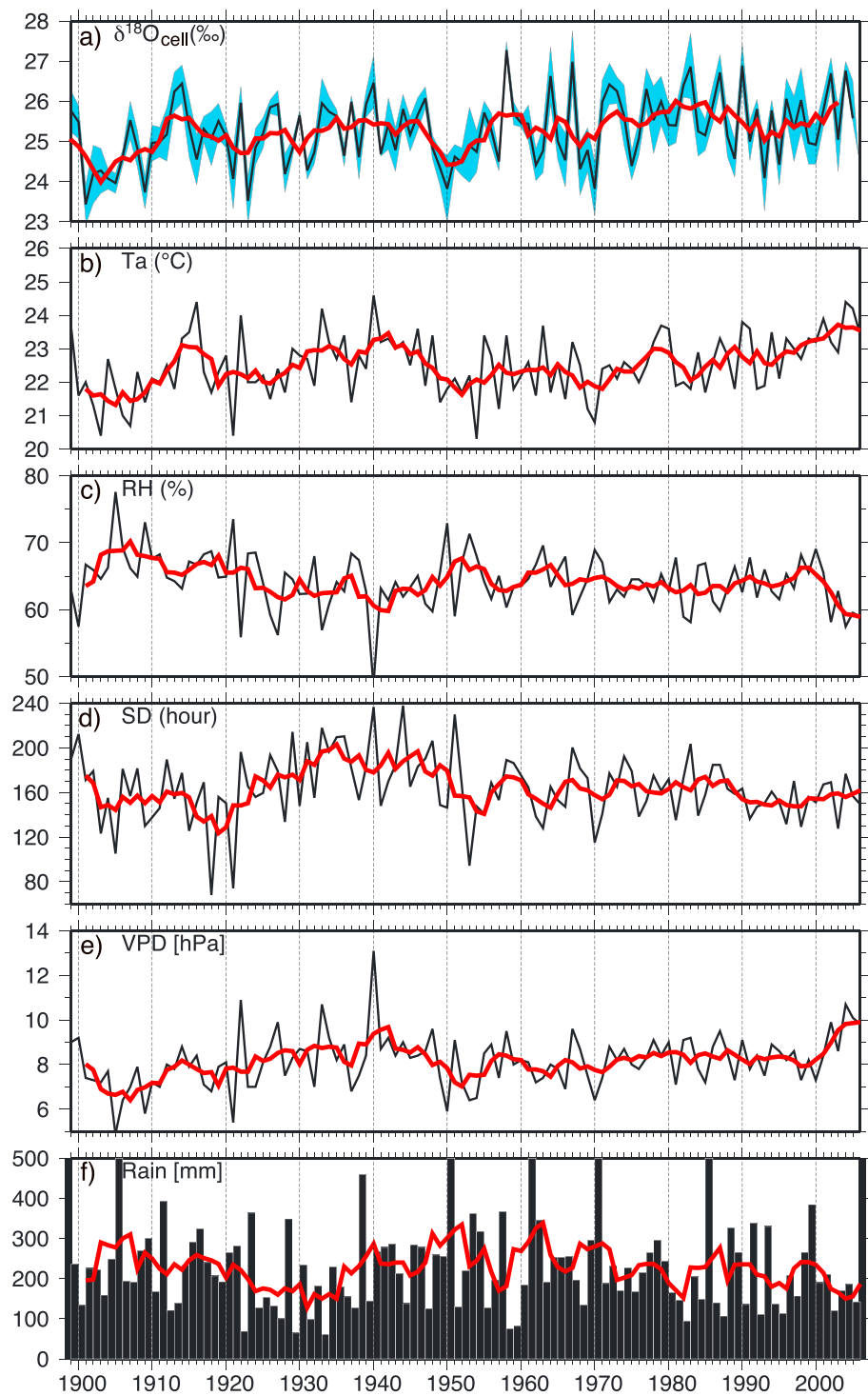


Figure 3. Time series of (a) the mean tree ring $\delta^{18}\text{O}$ chronology based on the four *Ch. obtusa* trees (solid lines) and their standard deviations (skyblue shading) and (b) the air temperature, (c) relative humidity, (d) sunshine duration, (e) vapor pressure deficit, and (f) precipitation in June (daytime means from 8:00 to 18:00) through the entire observation period at the meteorological observatory (Iida station). The solid red curves in Figures 3a–3f represent the 5 year running mean.

2.3. Isotope Data of Precipitation

Monthly records of the oxygen isotopic composition of rainfall at the Tokyo station (35.7°N, 139.8°E, 4 masl), 180 km to the east of the site, were obtained from the Global Network of Isotopes in Precipitation (GNIP). The observation was launched in March 1961 and stopped in December 1979. Tree ring sampling site (Agematsu) and GNIP Tokyo station are both located on the Pacific side of central Japan.

2.4. Meteorological Data

The nearest weather station using the Automated Meteorological Data Acquisition System (AMeDAS) is located in Nagiso town, 15 km south of the site. The AMeDAS station, however, only measures the temperature, precipitation, sunshine duration, and wind direction and speed. It also began collecting relatively recently, in 1979, far later than the manned stations, which began collecting data at the end of nineteenth century. In this study we therefore use meteorological data measured at a manned station. The nearest manned observatory is located in Iida city, 35 km southeast of the site (35.52°N, 137.82°E, 516 masl) across the north-south mountain range. Many meteorological variables (pressure, temperature, relative humidity, precipitation amount, sunshine duration, etc.) have been recorded since August of 1898. The year-to-year variations of the monthly mean temperature, precipitation amount, and sunshine duration observed at Iida station closely match those observed at Nagiso station over the period from 1979 to 2005. The Iida station archives hourly data at present but kept only 6-hourly data before the 1950s. The 6-hourly data were interpolated into hourly values. For this study we prepared hourly data from 1899 to 2005 and used it to calculate monthly daytime means from 8:00 to 18:00 as a boundary condition for the mechanistic model to backcalculate the oxygen isotopic composition of source water used by tree. Figure 3 shows the time series of the monthly means of the meteorological variables used in this study. To explore large-scale circulation and synoptic-scale weather conditions, we used 6-hourly data of a Japanese 55 year reanalysis (JRA-55) of the global atmosphere for 1958–2005 [Ebita *et al.*, 2011] and monthly mean data from the International Comprehensive Ocean-atmosphere Data Set (ICOADS) on oceanic cloudiness for 1979–2005 [Woodruff *et al.*, 2010]. The JRA-55 data and ICOADS data are on 1.25° × 1.25° and 2° × 2° horizontal grids, respectively. The onset record of Baiu rainfall in central Japan was obtained from the Japan Meteorological Agency website (www.jma.go.jp/jma/indexe.html). Several climate indices were used to examine the variability of the Baiu activity associated with atmospheric circulation changes on global scale. The Pacific-Japan (PJ) Index defined by Kubota *et al.* [2015], an index based on the difference in anomalies of the sea level pressure (SLP) at Yokohama, Japan, and Hengchun, Taiwan, was used as a marker of circulation anomalies on the tropical Pacific region. The Southern Oscillation Index (SOI) representing the standardized difference in SLP anomalies of Tahiti and Darwin [Ropelewski and Jones, 1987] was used as an indicator of the ENSO state. The North Atlantic Oscillation (NAO) index presenting the strength of the Icelandic low and the Azores high [Hurrell, 1995] was used as a marker of circulation anomalies in the Northern Hemisphere. The SOI and NAO data were obtained from the National Oceanic and Atmospheric Administration Earth System Research Laboratory website (<http://www.esrl.noaa.gov/psd>).

2.5. Mechanistic Modeling

In order to calculate the oxygen isotopic composition of source water, a mechanistic model predicting the oxygen isotopic composition of tree ring cellulose ($\delta^{18}\text{O}_{\text{cell}}$) was used in this study. This model consists of two components: (1) the physiological process controlling the changes in the oxygen isotopic composition of water as it moves through the plant and (2) the biogeochemical process governing the changes in the oxygen isotopic composition as it is incorporated into cellulose [e.g., Roden *et al.*, 2000; Barbour *et al.*, 2004; Barbour, 2007; Sternberg, 2008]. Physiologically, the source water taken up by the roots moves to the leaf and becomes enriched in the heavy $\delta^{18}\text{O}$ through evapotranspiration. Leaf water $\delta^{18}\text{O}$ enrichment above the source water (Δ_{es}) can be theoretically estimated based on the isotopic steady state model of leaf water [Craig and Gordon, 1965; Dongmann *et al.*, 1974; Farquhar *et al.*, 1993]:

$$\Delta_{\text{es}} = \epsilon_{\text{eq}} + \epsilon_{\text{k}} + (\delta^{18}\text{O}_{\text{atm}} - \delta^{18}\text{O}_{\text{source}} - \epsilon_{\text{k}}) e_{\text{a}}/e_{\text{i}} \quad (1)$$

where ϵ_{eq} is the equilibrium fractionation factor associated with the liquid to vapor phase change, ϵ_{k} is the kinetic fractionation associated with the diffusion of vapor into unsaturated air, $\delta^{18}\text{O}_{\text{atm}}$ and $\delta^{18}\text{O}_{\text{source}}$ are the isotopic compositions of the atmospheric vapor and source water (relative to V-SMOW), respectively, and $e_{\text{a}}/e_{\text{i}}$ is the ratio of ambient vapor pressure to that inside the leaf. ϵ_{eq} is calculated as a function of the leaf temperature T_{k} (K) [Bottinga and Craig, 1969].

$$\epsilon_{\text{eq}} = 2.644 - 3.206(10^3/T_{\text{k}}) + 1.534(10^6/T_{\text{k}}^2) \quad (2)$$

As shown in past study, the temperature can be assumed to be equal to the air temperature for needle-shaped leaves, because needles are closely coupled with the environment [Jones, 1992]. In this study, ambient air temperature (T_{air} (°C)) was used as $T_k - 273.15$, and thus, e_a/e_i was approximated with the relative humidity of the ambient air (h). Using the fractionation factor determined by Cappa [2003], ϵ_k is given by Farquhar *et al.* [1998]: $\epsilon_k = (32r_s + 21r_b)/(r_s + r_b)$, where r_s and r_b are the stomatal and boundary layer resistance to water vapor diffusion, respectively. Since r_b for needle-shaped leaves is negligible, we assumed $\epsilon_k = 32\text{‰}$ for our calculations.

Equation (1) predicts evaporative enrichment at the site of evaporation. Model predictions, however, often overestimate the actual enrichment of bulk leaf water due to the Péclet effect: the backward diffusion of enriched water into the leaf is opposed by the transpirational convection of unenriched water to the evaporating site [Farquhar and Lloyd, 1993]. Leaf water $\delta^{18}\text{O}$ enrichment above the source water (Δ_e) can be modeled from the Δ_{es} and the Péclet effect as follows:

$$\Delta_e = \Delta_{\text{es}}(1 - e^{-\wp})/\wp \quad (3)$$

where \wp is the dimensionless Péclet number, which is the ratio of advection of unenriched water to the site of evaporation, driven by transpiration, to back diffusion of the enriched water from the evaporation site:

$$\wp = LT_{\text{rans}}/CD \quad (4)$$

where L is the effective path length for water transport from the veins to the site of evaporation (m), T_{rans} is the transpiration rate ($\text{mol m}^{-2} \text{s}^{-1}$), C is the molar density of water ($55.5 \times 10^3 \text{ mol m}^{-3}$), and D is the diffusivity of H_2^{18}O in water ($\text{m}^2 \text{s}^{-1}$), which is temperature dependent [Cuntz *et al.*, 2007]. L is a variable parameter both within and between species. Song *et al.* [2013] recently found a significant negative power relationship between L and T_{rans} for white cedar ($L = 4.03 \times 10^{-4} T_{\text{rans}}^{-0.64}$; $R^2 = 0.370$). In this study, we assumed that this relationship can apply to the estimation of L for Japanese cypress.

Biochemically, the oxygen isotopic composition of photosynthetic products (sucrose) rises above that in leaf water as a result of biochemical fractionation, whereupon some of the oxygen atoms in the sucrose exchange with the source water to form cellulose, while the sucrose breaks down. Cellulose thus reflects both the exchange with enriched leaf water during sucrose synthesis and the exchange with the local source water during cellulose synthesis. The $\delta^{18}\text{O}$ enrichment of cellulose (Δ_{cell}) above the source water is given by [Barbour and Farquhar, 2000]:

$$\Delta_{\text{cell}} = \delta^{18}\text{O}_e(1 - p_{\text{ex}}p_x) + \epsilon_{\text{wc}} \quad (5)$$

where p_{ex} is the fraction of oxygen that has exchanged with the source water during cellulose synthesis and p_x is the unenriched source (xylem) water in the cell forming the cellulose. Cernusak *et al.* [2005] showed that p_{ex} varies in a range from 0.35 to 0.44, averaging about 0.40 under field conditions. Evidence suggests that p_x is close to unity ($p_x = 1$) for the cells in the source of mature trees [e.g., Roden *et al.*, 2000; Cernusak *et al.*, 2005]. The biochemical fractionation (ϵ_{wc}) between carbonyl oxygen and water is widely assumed to be 27‰ [e.g., Sternberg *et al.*, 1986; Yakir and DeNiro, 1990]. Using $\Delta_{\text{cell}} \approx \delta^{18}\text{O}_{\text{cell}} - \delta^{18}\text{O}_{\text{source}}$, equation (5) is converted to the δ notation:

$$\delta^{18}\text{O}_{\text{cell}} = \delta^{18}\text{O}_{\text{source}} + \Delta_e(1 - p_{\text{ex}}p_x) + \epsilon_{\text{wc}} \quad (6)$$

Equations (1), (3), and (6) are combined and solved for δ_{source} :

$$\delta^{18}\text{O}_{\text{source}} = \frac{\delta^{18}\text{O}_{\text{cell}} - f_d[\epsilon_{\text{eq}} + \epsilon_k + (\delta^{18}\text{O}_{\text{atm}} - \epsilon_k)h] - \epsilon_{\text{wc}}}{1 - f_d h} \quad (7)$$

where f_d is a dampening factor, which is defined by the following:

$$f_d = \Delta_e/\Delta_{\text{es}}(1 - p_{\text{ex}}p_x). \quad (8)$$

Equation (7) is similar to an equation presented by Saurer *et al.* [1997b] (see their equation 3), though they did not consider Péclet effect.

In order to back-calculate the $\delta^{18}\text{O}$ in precipitation ($\delta^{18}\text{O}_{\text{pr}}$) from the $\delta^{18}\text{O}_{\text{source}}$, we explored the relationship between the $\delta^{18}\text{O}_{\text{pr}}$ and $\delta^{18}\text{O}_{\text{source}}$. The $\delta^{18}\text{O}_{\text{source}}$ can be considered a mixture of the $\delta^{18}\text{O}_{\text{pr}}$ from shallower roots and $\delta^{18}\text{O}$ in deeper soil moisture from its deeper roots. The fraction of source water originating from the precipitation must respond to the dry-wet summer condition. A drier (rainier) summer condition, for example, may lead to a lower (higher) soil moisture content in the shallow root zone, indicating a lesser (greater) contribution of precipitation to the source water. From this, the difference between $\delta^{18}\text{O}_{\text{source}}$ and $\delta^{18}\text{O}_{\text{pr}}$ presumably depends on the total sunshine duration (SD) during the growing season as a proxy for drought. In this study, we used the following polynomial function to describe this dependence:

$$\delta^{18}\text{O}_{\text{source}} - \overline{\delta^{18}\text{O}_{\text{pr}}} = c_1\text{SD}^3 + c_2\text{SD}^2 + c_3\text{SD} + c_4 \quad (9)$$

where the $\overline{\delta^{18}\text{O}_{\text{pr}}}$ represents the precipitation-amount-weighted mean $\delta^{18}\text{O}_{\text{pr}}$ during the growing season and c_1 , c_2 , c_3 , and c_4 are empirically determined constants. These parameters were determined using observation data from 1962 to 1979, a period when the GNIP Tokyo station provided a continuous record of the monthly $\delta^{18}\text{O}$ in precipitation (hereafter, the “calibration period”).

2.6. Model Parameters

2.6.1. Atmospheric Vapor Oxygen Isotopes

The mean $\delta^{18}\text{O}$ in atmospheric vapor ($\delta^{18}\text{O}_{\text{atm}}$) during the growing season is required to calculate the $\delta^{18}\text{O}_{\text{source}}$ (equation (7)). Our early investigations of $\delta^{18}\text{O}_{\text{atm}}$ in central Japan showed a weak seasonality but a clear intraseasonal variability [Kurita *et al.*, 2013, 2015]. The temporal variability in $\delta^{18}\text{O}_{\text{atm}}$ reflects changes in weather conditions. When rain falls, a diffusive exchange takes place between raindrops and surrounding air and $\delta^{18}\text{O}_{\text{atm}}$ tends to decrease toward the isotopic equilibrium with precipitation. After the rainfall ends, $\delta^{18}\text{O}_{\text{atm}}$ tends to gradually increase and to remain at relatively high values on sunny days. These patterns suggest that the seasonal mean $\delta^{18}\text{O}_{\text{atm}}$ can be expressed as a time-weighted average function:

$$\delta^{18}\text{O}_{\text{atm}} = f_H \left(\overline{\delta^{18}\text{O}_{\text{pr}}} - \langle \epsilon_{\text{eq}} \rangle_{\text{rain}} \right) + (1 - f_H) \langle \delta^{18}\text{O}_{\text{atm}} \rangle_{\text{sunny}} \quad (10)$$

where f_H is the fraction of rainy days during the growing period, $\langle \epsilon_{\text{eq}} \rangle_{\text{rain}}$ represents the average ϵ_{eq} on rainy days, and $\langle \delta^{18}\text{O}_{\text{atm}} \rangle_{\text{sunny}}$ is the mean $\delta^{18}\text{O}_{\text{atm}}$ on sunny days. In this study the unknown parameter $\langle \delta^{18}\text{O}_{\text{atm}} \rangle_{\text{sunny}}$ was determined referring to continuous observation data collected at Nagoya University (96 km southwest of the sampling site) from June 2013 onward [Kurita *et al.*, 2015]. The mean value on nonprecipitating days in the growing season from 2013 to 2015 (-16.5 ± 2.0 ‰) was used for the calculation.

2.6.2. Transpiration Rate

The transpiration rate (T_{rans}) was estimated from the canopy stomatal conductance (g_s) and above-canopy atmospheric humidity deficit (D_o):

$$T_{\text{rans}} = g_s D_o / P_s \quad (11)$$

where P_s is the atmospheric pressure at the sampling site (875 hPa). In this study we ignore the daily variability of atmospheric pressure. The errors resulting from the use of a constant surface pressure value are negligible. As shown in past studies, g_s decreases exponentially as D_o increases [e.g., Jones, 1992]. We also know, however, that g_s varies linearly with D_o unless conditions are extremely dry. For coniferous trees, D_o can be identical to the vapor pressure deficit in air (VPD) since the canopy temperature is almost equal to the ambient temperature. Here g_s is expressed as a linear function with the monthly mean VPD:

$$g_s = c_5 \text{VPD} + c_6 \quad (12)$$

where c_5 and c_6 are the parameters of the experimentally determined linear relationship. These parameters were determined using monthly averaged data of T_{rans} and VPD observed in a coniferous forest (Japanese cedar) in Japan [Kumagai *et al.*, 2014]. A clear negative correlation can be found between g_s and VPD ($R^2 = 0.79$), with a small slope value ($-27 \text{ mmol m}^{-2} \text{ s}^{-1} \text{ kPa}^{-1}$). This is consistent with the results shown in Kumagai *et al.* [2008] based on rigorous calculations of canopy stomatal conductance. The relatively modest year-to-year variation of the monthly mean VPD in central Japan allowed us to set g_s as a constant ($80 \pm 8.0 \text{ mmol m}^{-2} \text{ s}^{-1}$).

Table 1. List of Constant Variables for the Model Calculation^a

Variable	Description	Value
ϵ_k	diffusive fractionation through stomata and air (‰)	32 (29–35)
ϵ_{wc}	fractionation between carbonyl oxygen and water (‰)	27 (24–30)
p_{ex}	fraction of exchangeable oxygen during cellulose synthesis	0.40 (0.36–0.44)
p_x	fraction of source water in xylem cell	1
$\langle \delta^{18}O_a \rangle_{sunny}$	mean $\delta^{18}O_{atm}$ on sunny days (‰)	-16.5 ± 2.0
g_s	canopy stomatal conductance ($mmol\ m^{-2}\ s^{-1}$)	80 ± 8.0
P_s	atmospheric pressure at the site (hPa)	875

^aThe values in parentheses indicate the range of uniform probability distribution for the Monte Carlo simulation.

2.7. Model Simulation

The constant parameters shown in Table 1 include unmeasured parameters that introduce potential error into the calculations. Differences between the $\delta^{18}O_{cell}$ values of the four trees are another source of uncertainty. Similar to Evans [2007], we use a Monte Carlo-based approach to assess these uncertainties. The $\delta^{18}O_{cell}$ and parameters are treated as independent random variables and sampled from a randomly perturbed probability density function of a uniform or Gaussian distribution over the plausible range of each value (see Table 1 for the parameters). The model was run more than 10,000 times with these random parameters. The calculated estimates were sorted, and then a mean and its 95% confidence interval for the output model were reported.

3. Results and Discussion

3.1. Growing Season

To determine the growing season of *Ch. obtusa* trees, we conducted a linear correlation analysis between $\delta^{18}O_{cell}$ and the monthly means of climate parameters. Based on equation (6), $\delta^{18}O_{cell}$ can be expressed as a function of air temperature (T_{air}), relative humidity (h), and $\delta^{18}O_{source}$. Table 2 shows the correlation coefficient (r) for $\delta^{18}O_{cell}$ against h and $\delta^{18}O_{pr}$ as a substitute for $\delta^{18}O_{source}$ for specified months during the calibration period (1962–1979). Given the weak variability of summer temperature, we chose not to investigate the dependence on T_{air} . The relative humidity is a main factor controlling the enrichment of heavy isotopes in leaf water. The magnitude of the enrichment increases as humidity decreases. As such, we expect to find a negative correlation between $\delta^{18}O_{cell}$ and humidity. Meanwhile, we predict a positive correlation between $\delta^{18}O_{cell}$ and $\delta^{18}O_{pr}$. The $\delta^{18}O_{cell}$ values in Table 2 show the highest positive correlation with $\delta^{18}O_{pr}$ ($r = 0.64$) and highest negative correlation with h ($r = -0.60$) in June. Both correlations are remarkably higher in June than in the other months, suggesting that the wood cellulose of a single year may largely reflect the environmental conditions in early summer (June) rather than those throughout the entire summer. The rainy season in central Japan usually starts from June and lasts to mid-July. The *Ch. obtusa* trees sampled for this study seemed to mainly grow during the rainy season.

3.2. Comparison of the Isotopic Composition of the Source Water and Precipitation

We compared the year-to-year isotopic variations in precipitation and in source water to explore the degree to which the $\delta^{18}O$ of the source water taken up from roots contained the precipitation isotope signal. Figure 4

Table 2. Correlation Coefficients (r) for the Oxygen Isotopic Compositions of Cellulose Against Relative Humidity (h) and Isotopic Compositions of Precipitation ($\delta^{18}O_{pr}$) for Specific Months During the Calibration Period

Month	$r(h)$	$r(\delta^{18}O_{pr})$
April	0.31 ^a	0.01
May	-0.41 ^a	0.41 ^a
June	-0.60 ^a	0.64 ^a
July	-0.02	0.44 ^a
August	0.01	0.22 ^a

^a p value < 0.1.

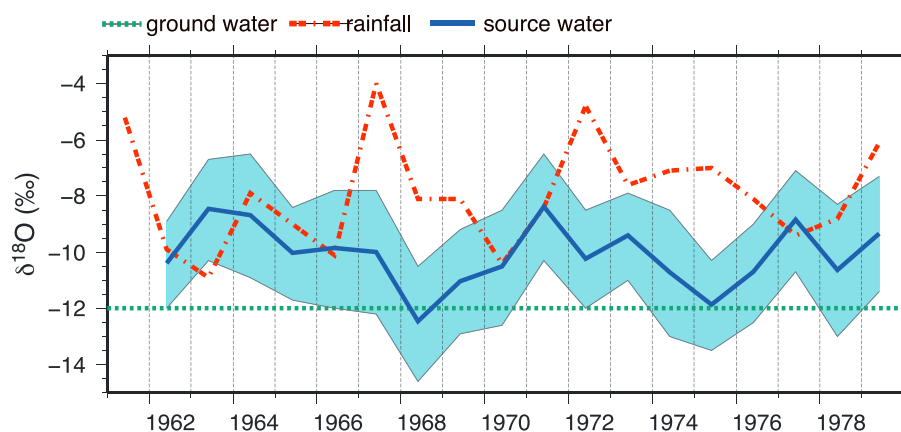


Figure 4. Comparison of the modeled $\delta^{18}\text{O}$ of source water (blue line) from the mechanistic model with the Monte Carlo estimate of the 95% confidence interval (skyblue shading) and the observed $\delta^{18}\text{O}$ of precipitation in June at GNIP Tokyo station (red dashed line). The green dotted line represents the $\delta^{18}\text{O}_{\text{gw}}$ values, which are recharged by rainfall at mountain peaks (see the text for details).

shows $\delta^{18}\text{O}_{\text{source}}$ time series values determined by a source water model (equation (7)) with a Monte Carlo estimate of the 95% confidence interval range, together with $\delta^{18}\text{O}_{\text{pr}}$ in June and $\delta^{18}\text{O}$ in water in the saturated zone (ground water) ($\delta^{18}\text{O}_{\text{gw}}$). The $\delta^{18}\text{O}_{\text{gw}}$ here corresponds to the most negative $\delta^{18}\text{O}$ of the soil water, which is recharged by rainfall at mountain peaks (1500 m above sea level). The climatological mean $\delta^{18}\text{O}$ value of rainfall at 1500 m height was estimated from the isotope map over central Japan [Yamanaka *et al.*, 2015]. Lacking a clear picture of the seasonality of $\delta^{18}\text{O}_{\text{pr}}$ in central Japan [Kurita *et al.*, 2015], we assumed that the interannual variability of $\delta^{18}\text{O}_{\text{gw}}$ was negligible. As Figure 4 shows, the $\delta^{18}\text{O}_{\text{source}}$ values move separately from the year-to-year variability of $\delta^{18}\text{O}_{\text{pr}}$ and lie between the values of $\delta^{18}\text{O}_{\text{pr}}$ and $\delta^{18}\text{O}_{\text{gw}}$, except for a few years. This suggests that the source water consists of a mixture of precipitation and groundwater. The surface soils during the rainy season are frequently supplied with precipitation, which may weaken the influence of the evaporative enrichment of the surface soil water. In the month of June, trees can be expected to take up precipitation relatively enriched in $\delta^{18}\text{O}$ via their shallow root system and to take up groundwater depleted of $\delta^{18}\text{O}$ via their deep root system. The fraction of precipitation to the source water may vary year-by-year, depending on environmental conditions such as the moisture content of the surface soil.

3.3. Relationship Between the Isotopic Composition of the Source Water and Precipitation

As mentioned above, the $\delta^{18}\text{O}_{\text{source}}$ can be considered as a mixture of the $\delta^{18}\text{O}_{\text{pr}}$ from shallower roots and the $\delta^{18}\text{O}$ in deeper soil moisture from deeper roots. The surface soil moisture may have a bearing on the fraction of source water originating from the precipitation. Lacking available data on the soil moisture at the site, we examined this relationship using the total sunshine duration (SD) in June as a proxy for the variability of the surface soil moisture during the growing season. As a rule of thumb, a longer (shorter) SD leads to increased (decreased) evaporation and decreased (increased) surface soil moisture. As expected, the difference between $\delta^{18}\text{O}_{\text{source}}$ and $\delta^{18}\text{O}_{\text{pr}}$ shows a clear negative correlation with SD (Figures 5 and 6). The maxima of difference between the $\delta^{18}\text{O}_{\text{source}}$ and $\delta^{18}\text{O}_{\text{pr}}$ values correspond to drought years when the sunshine duration far exceeds the mean value (160 h). By contrast, the $\delta^{18}\text{O}_{\text{source}}$ values are close to the $\delta^{18}\text{O}_{\text{pr}}$ values in years with shorter sunshine duration (wet conditions). The polynomial function shown in Figure 6 is equivalent to equation (9). Note that $\delta^{18}\text{O}_{\text{source}} - \delta^{18}\text{O}_{\text{pr}}$ has a clear negative correlation with SD than with the precipitation in June.

3.4. Modeling Oxygen Isotopic Compositions in Source Water

We applied the source water model (equation (7)) to the records of $\delta^{18}\text{O}_{\text{cell}}$ over the entire period with available meteorological data for June (1899–2005). Figure 7a exhibits an apparent interdecadal variation in the modeled $\delta^{18}\text{O}_{\text{source}}$ values, especially during the former half of the twentieth century. High $\delta^{18}\text{O}_{\text{source}}$ values are observed from the late 1900s to the mid-1920s, from the early 1950s to the late 1960s, and from the 1990s to the present, and the highest values fall in the 1990s. In contrast, low $\delta^{18}\text{O}_{\text{source}}$ values appear from the mid-1920 to the mid-1930 and from the late 1930s to the early 1950s, and the lowest values fall in the 1940s. These $\delta^{18}\text{O}_{\text{source}}$ fluctuations reflect the temporal variations in the precipitation [Endo, 2011] and SD in June (Figure 3d). The $\delta^{18}\text{O}_{\text{source}}$ values are most strongly corrected with SD ($r=0.75$, $p<0.001$). They are also

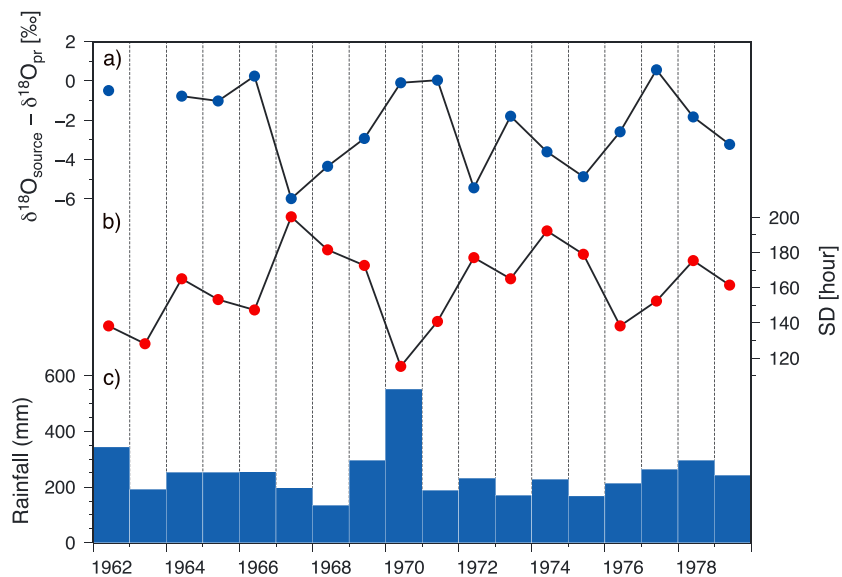


Figure 5. Interannual variations of (a) the difference between the observed $\delta^{18}\text{O}$ precipitation and modeled $\delta^{18}\text{O}$ of source water and (b) the sunshine duration, and (c) precipitation amount in June at the meteorological observatory during the calibration period.

significantly correlated with the rainfall amount ($r=0.41, p<0.01$) and the total rainfall hours in June ($r=0.62, p<0.001$), but the correlations are weaker than that with SD. Given that SD can be regarded as an indicator of the fraction of the source water originating from precipitation (Figure 6), the relative fraction of each water source (shallow versus deep soil water) might be the primary driver of the temporal variations in $\delta^{18}\text{O}_{\text{source}}$. Evaporation enhanced by the longer SD in the drier summer condition depletes the surface soil moisture, possibly inducing the trees to draw water preferentially from deeper soil layers. By contrast, a prolonged period of rainfall in wet years leads to increases the water percolation into the soil surface, possibly giving trees the opportunity to take up precipitated water from a surface root system. The explanation that the zone from which coniferous trees take up water changes between dry/wet soil conditions is consistent with a recent 2 year observation in Siberia showing that larch trees take up isotopically enriched water preferentially from the top soil (0–15 cm) in the wet summer condition [Saurer *et al.*, 2015]. In addition, the drier summer condition leads to a lower oxygen isotopic content of source water because of a lower (higher) fraction of top soil moisture (lower soil moisture) to the source water.

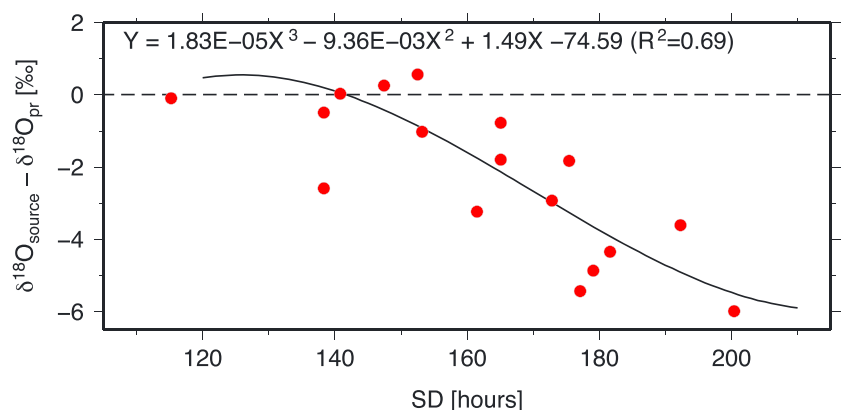


Figure 6. Difference between the $\delta^{18}\text{O}$ of precipitation and $\delta^{18}\text{O}$ of source water in relation to the sunshine duration in June during the calibration period. The solid line indicates the polynomial regression line. The right axis represents the fraction of precipitation to the source water.

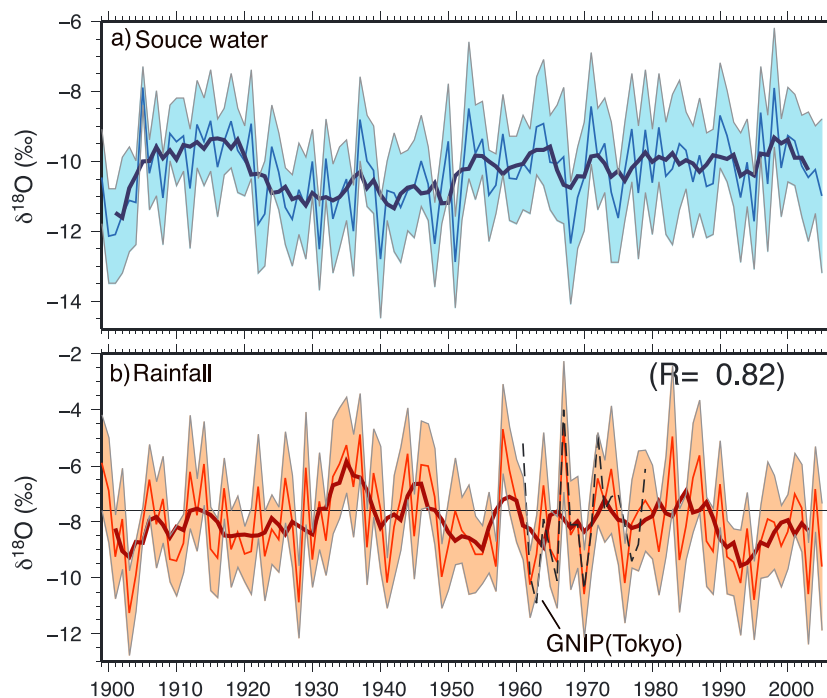


Figure 7. Modeled $\delta^{18}\text{O}$ of the (a) source water (blue line) from the mechanistic model and of (b) precipitation (red line) from the regression model during the entire record of the tree ring $\delta^{18}\text{O}$ over the period with available meteorological data (1898–2005). The shaded envelope represents the Monte Carlo estimate of the model error stemming from parameter uncertainty in the simulation. The solid thick lines represent the decadal component obtained by smoothing the series with a 5 year running mean filter. The dashed line is the $\delta^{18}\text{O}$ of June precipitation at GNIP Tokyo station (1962–1979).

3.5. Modeling Oxygen Isotopic Compositions in Precipitation

A 106 year long $\delta^{18}\text{O}_{\text{pr}}$ record is reconstructed using equation (9) (Figure 7b). The reconstructed $\delta^{18}\text{O}_{\text{pr}}$ values also exhibit interdecadal variability, reaching their highest values in the mid-1930s, but their interannual fluctuations are more considerable than those in $\delta^{18}\text{O}_{\text{source}}$. The amplitude of the year-to-year variability of $\delta^{18}\text{O}_{\text{pr}}$ is more than 2 times larger than that of $\delta^{18}\text{O}_{\text{source}}$. This variability is linked to changes in SD and relative humidity rather than changes in precipitation amount or temperature. The $\delta^{18}\text{O}_{\text{pr}}$ values in June at GNIP Tokyo showed a positive correlation with SD ($r=0.76, p<0.001$) and negative correlation with relative humidity ($r=-0.57, p<0.001$). The reconstructed $\delta^{18}\text{O}_{\text{pr}}$ values lie within the 90% of the prediction interval of the regression lines obtained from the GNIP Tokyo data (not shown). According to our early study Kurita *et al.* [2015], the interannual variability in $\delta^{18}\text{O}_{\text{pr}}$ at GNIP Tokyo station is driven by changes in the recurrence of synoptic-scale variations. As expected, synoptic-scale change over northeast Asia is the primary driver of interannual variations in the reconstructed $\delta^{18}\text{O}_{\text{pr}}$ during the period with available JRA-55 reanalysis data (1958–2005). Figure 8 shows composite maps of atmospheric circulation in June for years with high $\delta^{18}\text{O}_{\text{pr}}$ (anomalies from the mean of the whole period are higher than 1σ (1.5‰); 1958, 1967, 1974, 1983, and 1987 ($n=5$)) and years with low $\delta^{18}\text{O}_{\text{pr}}$ (anomalies are less than 1σ ; 1962, 1970, 1976, 1995, and 2003 ($n=5$)).

The mean position of the Baiu frontal zone identified as the region of higher cloudiness off the southern coast of Japan clearly differed between the years with high and low $\delta^{18}\text{O}_{\text{pr}}$. In years with low $\delta^{18}\text{O}_{\text{pr}}$, the Baiu frontal zone is situated along the southern coast of central Japan. In years with high $\delta^{18}\text{O}_{\text{pr}}$, the frontal zone shifts southward in association with the southward displacement of the Bonin high (BH). In June, the growing season, the Baiu frontal zone in central Japan migrates northward in association with seasonal intensification of the BH. The rainy season begins in around the middle of the month. Delays in the onset of the rainy season in some of the years with high $\delta^{18}\text{O}_{\text{pr}}$ result in reduced precipitation from the Baiu front, a condition corresponding to weak Baiu frontal activity.

Earlier we reported that the rainfall from the Baiu front is characterized by relatively lower $\delta^{18}\text{O}$ values than the other nonfrontal precipitation in summer [Kurita *et al.*, 2015], we speculated that the isotopic content of

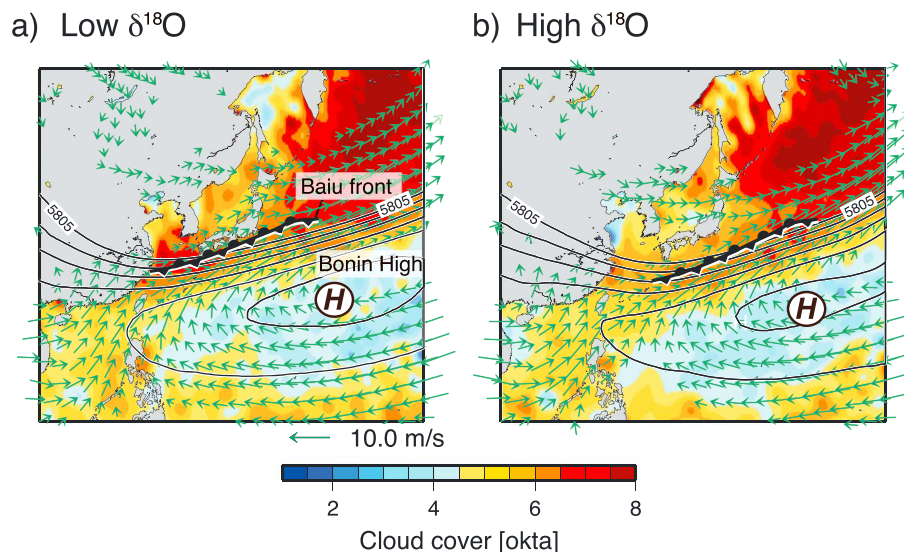


Figure 8. Composite maps of June mean cloud cover (shading: okta), geopotential height at 500 hPa (solid contours, contour interval 10 m), horizontal winds at 850 hPa (vectors: ms^{-1}) (a) in years with low $\delta^{18}\text{O}_{\text{pr}}$ (anomalies from the mean of the whole period are lower than 1σ) and (b) in years with high $\delta^{18}\text{O}_{\text{pr}}$ (anomalies are higher than 1σ). The June mean position of the Baiu frontal zone (represented by the stationary front symbol) is identified as the region of higher cloud cover off the southern coast of Japan.

June precipitation is higher (lower) in years when the rainy season begins late (early) than in a normal year. Further, we speculated that a delayed (early) onset of rainy season leads to an increase (decrease) in SD and a decrease (increase) in relative humidity. To verify these hypotheses, we examined the relationship between the fraction of the Baiu rainfall to the monthly rainfall (F_{br}) and $\delta^{18}\text{O}_{\text{pr}}$. The Baiu front is formed at the transition zone between the subtropical warm air mass and subpolar cold air mass. The Baiu rainfall corresponds to cold rainfall events associated with cyclonic or frontal systems. Following the approach of our earlier study, we divided daily precipitation at the observation site into rainfall from warm air mass and that from cold air mass using the calculated equivalent potential temperature (θ_e) for 1958–2005 [Kurita et al., 2015]. Then, we used synoptic charts to divide each event further into cyclonic/frontal rainfall, typhoon rainfall, and noncyclonic rainfall types. From 1958 to 2005, the F_{br} changes widely year by year, ranging from 0.10 to 0.97 (Figure 9). The reconstructed $\delta^{18}\text{O}_{\text{pr}}$ values exhibit a statistically robust decreasing trend as F_{br} increases ($r = -0.60, p < 0.001$).

We also found a significant negative correlation between the reconstructed $\delta^{18}\text{O}_{\text{pr}}$ and the the onset days ($r = 0.38, p < 0.01$) during the same analysis period (1958–2005). Figure 10 shows the time series of anomalies of the $\delta^{18}\text{O}_{\text{pr}}$ and the onset days from the average between 1958 and 1972. The onset days tend to significantly decrease in the latter half of the twentieth century ($p = 0.034$). Despite large uncertainty in the $\delta^{18}\text{O}_{\text{pr}}$ (see Figure 7b), a long-term decreasing trend was also found in the mean values of $\delta^{18}\text{O}_{\text{pr}}$ ($p = 0.21$). Judging from these findings, the reconstructed $\delta^{18}\text{O}_{\text{pr}}$ shows strong potential for use as an indicator of the Baiu rainband activity in central Japan.

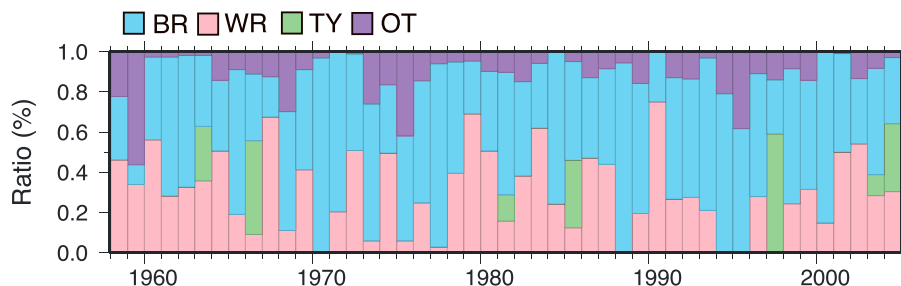


Figure 9. Relative contribution of each type of rainfall to monthly rainfall in June at the observation site. Rainfall is classified into five types: Baiu rainfall (BR), warm rainfall (WR), typhoon rainfall (TY), and others (OT).

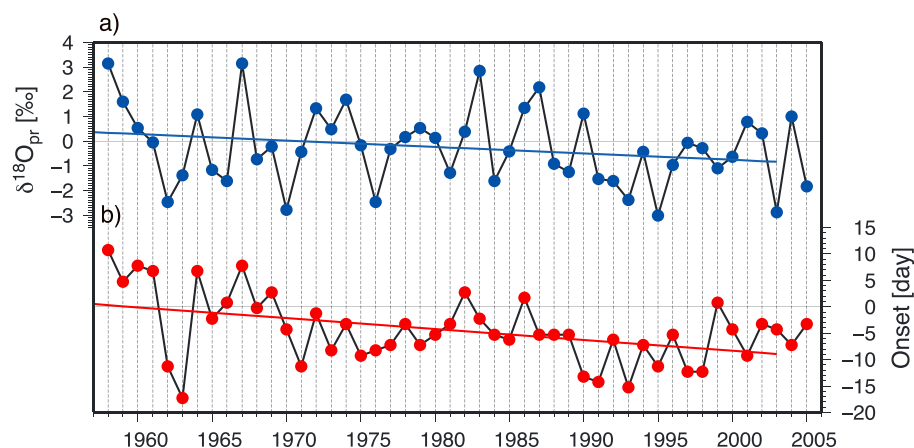


Figure 10. Time series of anomalies of (a) modeled $\delta^{18}\text{O}$ in June precipitation and (b) rainy season onset days in central Japan over the period with available onset records (1958–2005). Anomalies are relative to the 1958–1972 base period mean. The straight lines are the best linear fits (trend lines).

3.6. Climate Drivers of Interannual to Decadal Variation in Baiu Rainband Activity

The position of the Baiu frontal zone is anchored by the midtropospheric warm advection [Sampe and Xie, 2010]. The interannual variations in the Baiu frontal zone are mainly controlled by the variations in the atmospheric circulation pattern that change the midtropospheric warm advection [Kosaka et al., 2011]. The PJ teleconnection pattern, for example, is a circulation anomaly pattern with a dominant influence on the Baiu frontal activity. Through a PJ teleconnection, enhanced (weakened) convective activity over the east of Philippines leads to anomalous intensification (weakening) of the BH and subsequently to decreased (increased) Baiu rainfall in Japan [e.g., Nitta, 1987; Kosaka and Nakamura, 2006].

Figure 11a exhibits the regressed pattern of geopotential height anomalies (GPH) at 500 hPa with the reconstructed $\delta^{18}\text{O}_{\text{pr}}$ for the years in recent decades (1979–2005) when the PJ pattern dominates (PJ summer). In this study we define PJ summer events when the PJ index of a summer exceeds 1σ ($|PJ| \geq 1$). As expected, GPH anomalies exhibit a PJ-like meridional dipole pattern over the NWP. Note that this anomalous dipole extends into the lower troposphere (not shown). Positive GPH anomalies covering the NWP, however, are shifted eastward from Japan. In contrast, positive GPH anomalies zonally extended from northeast China, and Japan corresponds to a wave train-like anomalies along the Asian jet (40°N) over the Eurasian continent. This wave train originates from the Europe and propagates toward East Asia. This feature is similar to that of the Silk Road pattern, another of the major teleconnection patterns that influence the precipitation in Japan in early summer [Enomoto et al., 2003; Enomoto, 2004; Kosaka et al., 2009]. In the case of PJ summer, the interannual variability of the Baiu frontal activity in early summer may be linked to the variability of atmospheric circulation elicited by the Silk Road teleconnection patterns. For the summer with a negative PJ pattern (cyclonic anomalies over the east of the Philippines), cyclonic anomalies over the northeast Asia are induced remotely through the Silk Road teleconnection patterns. The anomalous cyclonic activity corresponds to decreased $\delta^{18}\text{O}_{\text{pr}}$ values, reflecting increase of the Baiu rainfall in early summer [Krishnan and Sugi, 2001; Kosaka et al., 2011]. During the summer with a positive PJ pattern (anticyclonic anomalies over the east of the Philippines), by contrast, anticyclonic anomalies over the region are associated with a weakening of the Baiu activity and subsequent dry summer characterized by high $\delta^{18}\text{O}_{\text{pr}}$ values.

In non-PJ summer ($|PJ| < 1$), we find no obvious meridional dipole of the PJ-like pattern or wavelike anomalies along the Asian jet (Figure 11b). Meanwhile, we see wave train-like anomalies across Siberia along the polar front jet (60°N – 70°N). This wave train pattern is identical with the Rossby wave propagation leading to the formation of the Okhotsk high, a cold high over the Okhotsk Sea, in early summer [Nakamura and Fukumachi, 2004]. The strength of the Okhotsk high varies widely from year to year. Intensifications of the Okhotsk high (anticyclonic anomalies) bring anomalous cool northeastlies to northeastern Japan [Shimada et al., 2014], thereby increasing the Baiu precipitation in Japan [Wang, 1992]. For the non-PJ summer, the development of the Okhotsk high seems to be a key contributor to the interannual variability of the Baiu frontal activity in central Japan from 1979 to 2005. A wave train pattern across northern Siberia can be seen in the regression map between the GPH at 500 hPa in June and the winter NAO index [Ogi et al., 2003, 2004]. Ogi et al. [2003, 2004]

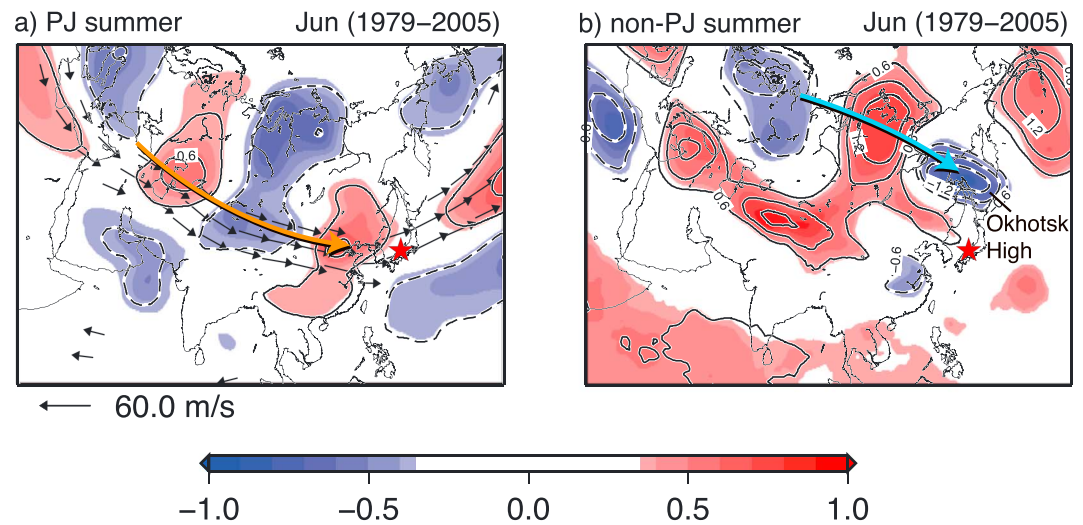


Figure 11. The 500 hPa geopotential height anomalies in June regressed against the tree ring reconstructed $\delta^{18}\text{O}$ in June precipitation in central Japan in years with PJ summer (1980, 1981, 1985, 1986, 1987, 1988, 1991, 1996, 1998, 2003, 2004, and 2005 ($n = 12$)) and years with (b) non-PJ summer (1979, 1982, 1992, 1994, 1997, 1999, 2000, 2001, and 2002 ($n = 9$)). Color shading represents a significance level of less than 20% based on the t statistic. The contour interval is 0.3, with solid and dashed lines indicating anomalous circulation, respectively. The arrow in Figure 11a indicates the 500 hPa horizontal wind in June in the Asian jet region. The red star represents the sampling site.

proposed that sea ice, surface snow, and sea surface temperature (SST) anomalies attributed to the winter variability of the NAO generate this wave train pattern propagating to the Okhotsk Sea and exert substantial influence on the Okhotsk high in the subsequent early summer. *Ogi et al.* [2004] also reported that the Okhotsk high in June is strong (weak) when the NAO index of the previous winter is in a positive (negative) phase. We thus expect that the Baiu frontal activity in central Japan positively correlates with the winter NAO index. So that the $\delta^{18}\text{O}_{\text{pr}}$ must negatively correlate with the winter NAO index.

Next, we examined whether these external forcing mechanisms persist through early summer before 1979. Figure 12 exhibits a time series of the moving correlation of the reconstructed $\delta^{18}\text{O}_{\text{pr}}$ with the PJ and the winter NAO indices during the whole of the twentieth century. The above mentioned positive correlation with the PJ index and negative correlation with the winter NAO is apparent from the late 1980s onward. These relationships, however, change abruptly in the 1980s and remain unclear until the mid-1950s. During the years 1958–1976, the regression of June GPH anomalies at 500 hPa against the reconstructed $\delta^{18}\text{O}_{\text{pr}}$ exhibits no remotely forced anomalous circulation patterns but manifests anticyclonic anomalies near the center position of the BH (not shown). The Baiu rainfall in central Japan in this period may reflect the intensification/weakening of the BH. This is consistent with the relation found between the BH activity and the year-to-year variability of summer $\delta^{18}\text{O}_{\text{pr}}$ observed at GNIP Tokyo (1962–1979) [*Kurita et al.*, 2015].

Before the mid-1950s, $\delta^{18}\text{O}_{\text{pr}}$ was negatively correlated with the winter NAO, which remained significant at the 80% confidence level for all periods except for the 1930–1940s. The periods of negative $\delta^{18}\text{O}_{\text{pr}}$ -NAO correlations correspond well to period of the persistent positive NAO in the preceding winter (Figure 12c). This finding is consistent with the fact that the atmospheric blocking events that lead to the prolonged appearance of the Okhotsk high occur in summer after the positive NAO winter [*Ogi et al.*, 2003]. During the exceptional period (1930–1940s), the correlation between the $\delta^{18}\text{O}_{\text{pr}}$ and PJ index is significant. We were interested to observe that the positive $\delta^{18}\text{O}_{\text{pr}}$ -PJ correlation only appears during the period when the PJ index is correlated with ENSO in the preceding winter (Figure 12b). In addition, the periods of ENSO-PJ correlation (1930–1940s and 1980–1990s) roughly coincide with the periods when the SST anomalies induced by ENSO are observed in the northern Indian Ocean during boreal summer [*Kubota et al.*, 2015]. These findings imply that the $\delta^{18}\text{O}_{\text{pr}}$ -PJ relationship is clearly seen during the periods when the “Indian Ocean capacitor effect” is active: warm SST anomalies in the tropical Indian Ocean after El Niño triggers an anomalous anticyclonic circulation over the east of Philippines (negative PJ pattern) and eventually intensify the Meiyu-Baiu frontal activity [*Xie et al.*, 2009]. The interannual variability of Baiu rainfall in central Japan is associated with several teleconnection

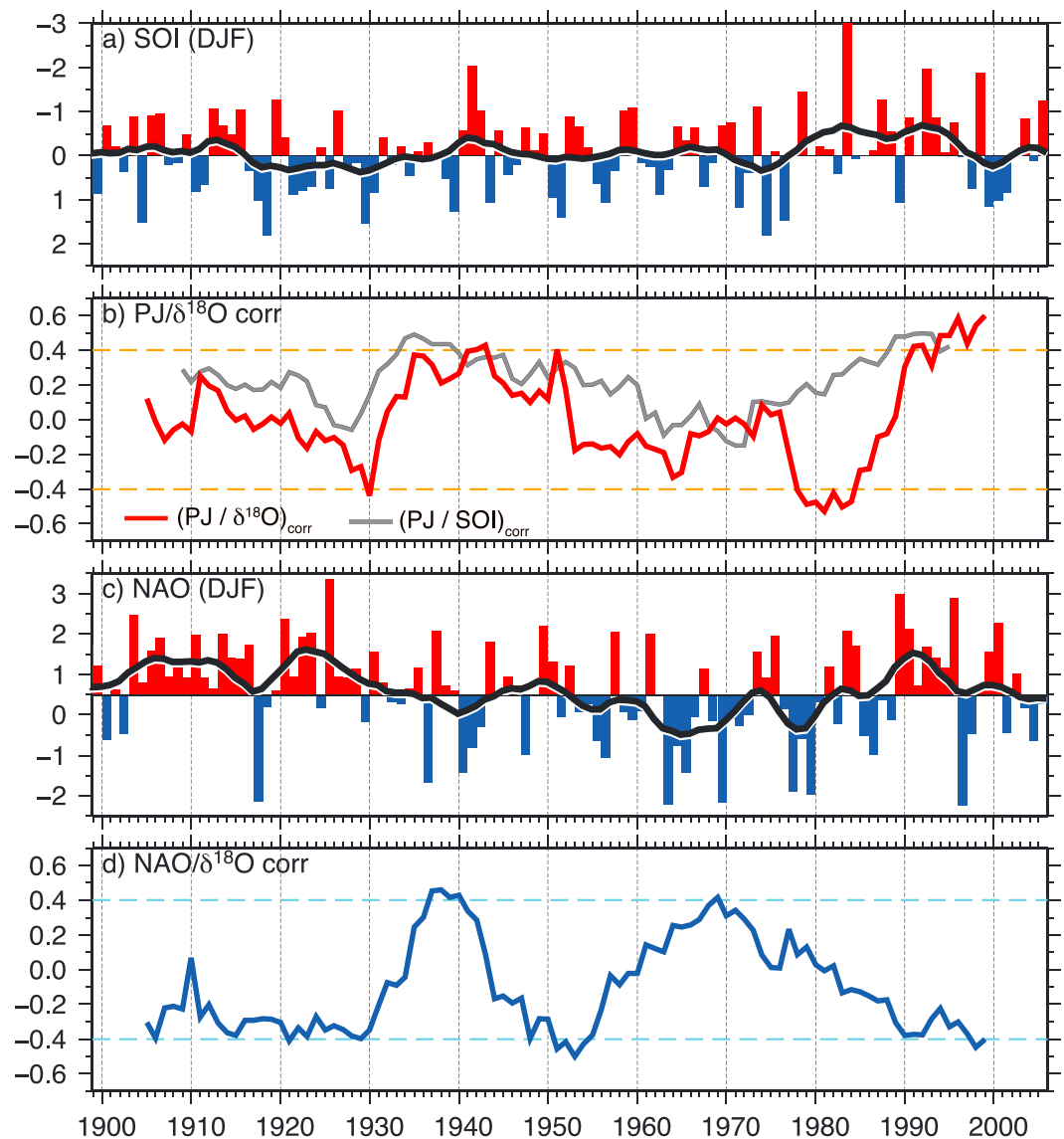


Figure 12. (a and c) Time series of the winter (December to subsequent February) mean SOI index (Figure 12a) and NAO index (Figure 12c) with the 11 year moving average (tick black line) from 1899 to 2005. (b and d) The 11 year running correlations of the reconstructed $\delta^{18}\text{O}$ in June precipitation in central Japan with the PJ index (Figure 12c) red line), and (Figure 12 the winter NAO index (Figure 12c) (blue line). The 11 year running correlations between the PJ index, and winter mean SOI index (gray line) are also shown in Figure 12c. Dashed lines represent significance levels of less than 20%.

patterns. But, rather than exerting a permanent influence on the Baiu rainfall, these external forcing mechanisms vary from a decadal to multidecadal time scale.

4. Conclusions

We reconstructed the 106 year long oxygen isotopic composition of precipitation ($\delta^{18}\text{O}_{pr}$) during early summer rainy season (June) in central Japan by determining the oxygen isotopic composition tree rings from the region. The year-to-year variability of the reconstructed $\delta^{18}\text{O}_{pr}$ reflected the interannual variability of summer precipitation associated with the Baiu rainband, a part of the EASM. The variability of the reconstructed $\delta^{18}\text{O}_{pr}$ in the most recent 25 years was closely linked to external forcing mechanisms such as the PJ pattern, the Silk Road pattern, and a wave train pattern along the polar jet. These teleconnection patterns are consistent with the climate drivers affecting the Baiu variability [Kosaka *et al.*, 2011]. However, the 106 year long $\delta^{18}\text{O}_{pr}$ reveals that the external forcing mechanisms shown in recent decades do not persist through the last

twentieth century. From the 1950s to 1980s, local factors such as anomalous intensification/weakening of the BH are dominant causes of the interannual variability of the $\delta^{18}\text{O}_{\text{pr}}$. Before the 1950s, the $\delta^{18}\text{O}_{\text{pr}}$ variability is closely related to climate variability in the preceding winter. Over the period when the positive NAO persists during the preceding winter (1910s–1930s and 1940s–1950s), the $\delta^{18}\text{O}_{\text{pr}}$ shows a negative correlation with the winter NAO, indicating that a wave train pattern along the polar jet contributes to the variability of the Baiu rainband. Meanwhile, when the PJ index is significantly correlated with ENSO in the preceding winter (1930s–1940s), $\delta^{18}\text{O}_{\text{pr}}$ values are positively correlated with the PJ index, indicating that ENSO is major driver of the variability of the Baiu rainband. These interdecadal modulations suggest that natural decadal variability may be the primary driver of the variability of the Baiu rainband through the last twentieth century, rather than anthropogenically forced changes.

Acknowledgments

This study was supported by Research Project No. H-05 of the Research Institute for Humanity and Nature (RIHN), entitled “Societal Adaptation to Climate Change: Integrating Paleo-climatological Data with Historical and Archaeological Evidences” (PI: Takeshi Nakatsuka). The model calculations were performed with the computational resources of the National Institute for Environmental Studies (NIES). We gratefully acknowledge Li Zhen for performing the oxygen isotope analysis and Hisayuki Kubota for providing the PJ index data. The comments from Masaki Sano and Hiroyuki Kitagawa on dendrochronology and isotope analysis were very helpful for this study. Last, we convey a special note of thanks to a reviewer, Louis Scuderi, and an anonymous reviewer for offering constructive comments and suggestions in a review of an earlier version of this manuscript. The data are available as indicated in section 2 and otherwise from the authors upon request (nkurita1126@nifty.com).

References

- Anderson, W. T., S. M. Bernasconi, J. A. McKenzie, M. Saurer, and F. Schweingruber (2002), Model evaluation for reconstructing the oxygen isotopic composition in precipitation from tree ring cellulose over the last century, *Chem. Geol.*, *182*(2), 121–137.
- Barbour, M. M. (2007), Stable oxygen isotope composition of plant tissue: A review, *Funct. Plant Biol.*, *34*(2), 83–94, doi:10.1071/FP06228.
- Barbour, M. M., and G. D. Farquhar (2000), Relative humidity-and ABA-induced variation in carbon and oxygen isotope ratios of cotton leaves, *Plant Cell Environ.*, *23*(5), 473–485.
- Barbour, M. M., J. S. Roden, G. D. Farquhar, and J. R. Ehleringer (2004), Expressing leaf water and cellulose oxygen isotope ratios as enrichment above source water reveals evidence of a Péclet effect, *Oecologia*, *138*(3), 426–435, doi:10.1007/s00442-003-1449-3.
- Bottinga, Y., and H. Craig (1969), Oxygen isotope fractionation between CO_2 and water, and the isotopic composition of marine atmospheric CO_2 , *Earth Planet. Sci. Lett.*, *5*, 285–295, doi:10.1016/s0012-821x(68)80054-8.
- Brienen, R. J., G. Helle, T. L. Pons, J.-L. Guyot, and M. Gloor (2012), Oxygen isotopes in tree rings are a good proxy for Amazon precipitation and El Niño–Southern oscillation variability, *Proc. Natl. Acad. Sci.*, *109*(42), 16,957–16,962, doi:10.1073/pnas.1205977109.
- Brienen, R. J. W., P. Hietz, W. Wanek, and M. Gloor (2013), Oxygen isotopes in tree rings record variation in precipitation $\delta^{18}\text{O}$ and amount effects in the south of Mexico, *J. Geophys. Res. Biogeosci.*, *118*(4), 1604–1615, doi:10.1002/2013JG002304.
- Cappa, C. D. (2003), Isotopic fractionation of water during evaporation, *J. Geophys. Res.*, *108*(D16), 4525–10, doi:10.1029/2003JD003597.
- Cernusak, L. A., G. D. Farquhar, and J. S. Pate (2005), Environmental and physiological controls over oxygen and carbon isotope composition of Tasmanian blue gum, *Eucalyptus globulus*, *Tree Physiol.*, *25*(2), 129–146.
- Craig, H., and L. I. Gordon (1965), Deuterium and oxygen-18 variations in the ocean and the marine atmosphere, in *Stable Isotopes in Oceanographic Studies and Palaeotemperatures*, edited by E. Tongiorgi, pp. 9–130, Naz. delle Ric., Pisa, Italy.
- Cuntz, M., J. Ogé, G. D. Farquhar, P. Peylin, and L. A. Cernusak (2007), Modelling advection and diffusion of water isotopologues in leaves, *Plant Cell Environ.*, *30*(8), 892–909, doi:10.1111/j.1365-3040.2007.01676.x.
- Danis, P. A., V. Masson-Delmotte, M. Stievenard, M. T. Guillemain, V. Daux, P. Naveau, and U. von Grafenstein (2006), Reconstruction of past precipitation $\delta^{18}\text{O}$ using tree-ring cellulose $\delta^{18}\text{O}$ and $\delta^{13}\text{C}$: A calibration study near Lac d’Annecy, France, *Earth and Planet. Sci. Lett.*, *243*(3–4), 439–448, doi:10.1016/j.epsl.2006.01.023.
- Dongmann, D. G., H. W. Nürnberg, H. Förstel, and K. Wagener (1974), On the enrichment of H_2^{18}O in the leaves of transpiring plants, *Radiat. Environ. Biophys.*, *11*(1), 41–52, doi:10.1007/BF01323099.
- Ebita, A., et al. (2011), The Japanese 55-year reanalysis “JRA-55”: An interim report, *Sci. Online Lett. Atmos.*, *7*, 149–152, doi:10.2151/sola.2011-038.
- Edwards, T., and P. Fritz (1986), Assessing meteoric water composition and relative humidity from ^{18}O and ^2H in wood cellulose: Paleoclimatic implications for Southern Ontario, Canada, *Appl. Geochem.*, *1*(6), 715–723, doi:10.1016/0883-2927(86)90093-4.
- Endo, H. (2011), Long-term changes of seasonal progress in Baiu rainfall using 109 years (1901–2009) daily station data, *Sci. Online Lett. Atmos.*, *7*, 5–8, doi:10.2151/sola.2011-002.
- Enomoto, T. (2004), Interannual variability of the Bonin high associated with the propagation of Rossby waves along the Asian jet, *J. Meteorol. Soc. Jpn.*, *82*(4), 1019–1034, doi:10.2151/jmsj.2004.1019.
- Enomoto, T., B. J. Hoskins, and Y. Matsuda (2003), The formation mechanism of the Bonin high in August, *Q. J. R. Meteorol. Soc.*, *129*(587), 157–178, doi:10.1256/qj.01.211.
- Evans, M. N. (2007), Toward forward modeling for paleoclimatic proxy signal calibration: A case study with oxygen isotopic composition of tropical woods, *Geochem. Geophys. Geosyst.*, *8*(7), Q07008, doi:10.1029/2006GC001406.
- Farquhar, G. D., and J. Lloyd (1993), Carbon and oxygen isotope effects in the exchange of carbon dioxide between terrestrial plants and the atmosphere, in *Stable Isotopes and Plant Carbon-Water Relations*, edited by A. H. J. R. Ehleringer, and G. Farquhar, pp. 47–70, Acad. Press, San Diego.
- Farquhar, G. D., J. Lloyd, J. A. Taylor, L. B. Flanagan, J. P. Syvertsen, K. T. Hubick, S. C. Wong, and J. R. Ehleringer (1993), Vegetation effects on the isotope composition of oxygen in atmospheric CO_2 , *Nature*, *363*(6428), 439–443.
- Farquhar, G. D., M. M. Barbour, and B. K. Henry (1998), Interpretation of oxygen isotope composition of leaf material, in *Stable Isotopes: Integration of Biological, Ecological and Geochemical Processes*, edited by H. Griffiths, pp. 27–62, BIOS Sci., Oxford, England.
- Gemmer, M., B. Su, and T. Jiang (2012), Water resources under climate change in the Yangtze River basin, in *Climatic Change and Global Warming of Inland Waters: Impacts and Mitigation for Ecosystems and Societies*, edited by C. R. Goldman, M. Kumagai, and R. D. Roberts, John Wiley, Ltd, Chichester, U. K., doi:10.1002/9781118470596.ch5.
- Harada, M., Y. Watanabe, T. Nakatsuka, S. Tazuru-Mizuno, Y. Horikawa, and J. Sugiyama (2014), Alpha-cellulose extraction procedure for the tropical tree sungkai (*Peronema canescens* Jack) by using an improved vessel for reliable paleoclimate reconstruction, *Geochem. J.*, *48*, 299–307.
- Hurrell, J. W. (1995), Decadal trends in the north atlantic oscillation: Regional temperatures and precipitation, *Science*, *269*(5224), 676–679, doi:10.1126/science.269.5224.676.
- Jones, H. G. (1992), *Plants and Microclimate: A Quantitative Approach to Environmental Plant Physiology*, 428 pp., Cambridge Univ. Press, Cambridge, U. K.
- Kagawa, A., M. Sano, T. Nakatsuka, T. Ikeda, and S. Kubo (2015), An optimized method for stable isotope analysis of tree rings by extracting cellulose directly from cross-sectional laths, *Chem. Geol.*, *393–394*, 16–25.

- Kosaka, Y., and H. Nakamura (2006), Structure and dynamics of the summertime Pacific Japan teleconnection pattern, *Q. J. R. Meteorol. Soc.*, *132*, 2009–2030, doi:10.1256/qj.05.204.
- Kosaka, Y., H. Nakamura, M. Watanabe, and M. Kimoto (2009), Analysis on the dynamics of a wave-like teleconnection pattern along the summertime Asian jet based on a reanalysis dataset and climate model simulations, *J. Meteorol. Soc. Jpn*, *87*(3), 561–580, doi:10.2151/jmsj.87.561.
- Kosaka, Y., S.-P. Xie, and H. Nakamura (2011), Dynamics of interannual variability in summer precipitation over East Asia, *J. Clim.*, *24*(20), 5435–5453, doi:10.1175/2011JCLI4099.1.
- Krishnan, R., and M. Sugi (2001), Baiu rainfall variability and associated monsoon teleconnections, *J. Meteorol. Soc. Jpn*, *79*(3), 851–860, doi:10.2151/jmsj.79.851.
- Kubota, H., Y. Kosaka, and S.-P. Xie (2015), A 117-year long index of the Pacific-Japan pattern with application to interdecadal variability, *Int. J. Climatol.*, *36*(4), 1575–1589, doi:10.1002/joc.4441.
- Kumagai, T., M. Tateishi, T. Shimizu, and K. Otsuki (2008), Transpiration and canopy conductance at two slope positions in a Japanese cedar forest watershed, *Agric. For. Meteorol.*, *148*(10), 1444–1455, doi:10.1016/j.agrformet.2008.04.010.
- Kumagai, T., M. Tateishi, Y. Miyazawa, M. Kobayashi, N. Yoshifuji, H. Komatsu, and T. Shimizu (2014), Estimation of annual forest evapotranspiration from a coniferous plantation watershed in Japan (1): Water use components in Japanese cedar stands, *J. Hydrol.*, *508*, 66–76, doi:10.1016/j.jhydrol.2013.10.047.
- Kurita, N., Y. Fujiyoshi, R. Wada, T. Nakayama, Y. Matsumi, T. Hiayama, and K. Muramoto (2013), Isotopic variations associated with north-south displacement of the Baiu front, *Sci. Online Lett. Atmos.*, *9*, 187–190, doi:10.2151/sola.2013-042.
- Kurita, N., Y. Fujiyoshi, T. Nakayama, Y. Matsumi, and H. Kitagawa (2015), East Asian monsoon controls on the inter-annual variability in precipitation isotope ratio in Japan, *Clim. Past*, *11*(2), 339–353, doi:10.5194/cp-11-339-2015.
- Loader, N., I. Robertson, A. C. Barker, V. Switsur, and J. Waterhouse (1997), An improved technique for the batch processing of small wholewood samples to α -cellulose, *Chem. Geol.*, *136*, 313–317.
- Miller, D. L., C. I. Mora, H. D. Grissino-Mayer, C. J. Mock, M. E. Uhle, and Z. Sharp (2006), Tree-ring isotope records of tropical cyclone activity, *Proc. Natl. Acad. Sci.*, *103*(39), 14,294–14,297, doi:10.1073/pnas.0606549103.
- Mitsutani, T. (1987a), Establishment and application of dendrochronology in Japan. I Characteristics of ring patterns in modern Hinoki (*Chamaeyparis obtusa* S. et Z) trees, *J. Jpn Wood Res. Soc.*, *33*(3), 165–174.
- Mitsutani, T. (1987b), Establishment and application of dendrochronology in Japan. II. Correlation analysis of ring patterns among hinoki trees from different sites and between hinoki and other species, *J. Jpn Wood Res. Soc.*, *33*(3), 175–181.
- Nakamura, H., and T. Fukamachi (2004), Evolution and dynamics of summertime blocking over the Far East and the associated surface Okhotsk high, *Q. J. R. Meteorol. Soc.*, *130*(5), 1213–1233, doi:10.1256/qj.03.101.
- Ninomiya, K., T. Murakami, C. P. Chang, and T. N. Krishnamurti (1987), The early summer rainy season (Baiu) over Japan, in *Monsoon Meteorol.*, pp. 93–121, Oxford Univ. Press, New York.
- Nitta, T. (1987), Convective activities in the tropical western Pacific and their impact on the Northern Hemisphere summer circulation, *J. Meteorol. Soc. Jpn*, *65*(3), 373–390.
- Ogi, M., Y. Tachibana, and K. Yamazaki (2003), Impact of the wintertime North Atlantic Oscillation (NAO) on the summertime atmospheric circulation, *Geophys. Res. Lett.*, *30*(1), 1704–1, doi:10.1029/2003GL017280.
- Ogi, M., Y. Tachibana, and K. Yamazaki (2004), The connectivity of the winter North Atlantic Oscillation (NAO) and the summer Okhotsk High, *J. Meteorol. Soc. Jpn*, *82*(3), 905–913, doi:10.2151/jmsj.2004.905.
- Roden, J., G. Lin, and J. R. Ehleringer (2000), A mechanistic model for interpretation of hydrogen and oxygen isotope ratios in tree-ring cellulose, *Geochim. Cosmochim. Acta*, *64*, 21–35, doi:10.1016/S0016-7037(99)00195-7.
- Ropelewski, C. F., and P. D. Jones (1987), An extension of the Tahiti-Darwin Southern Oscillation Index, *Mon. Weather Rev.*, *115*(9), 2161–2165, doi:10.1175/1520-0493(1987)115<2161:aeotts>2.0.co;2.
- Sampe, T., and S.-P. Xie (2010), Large-scale dynamics of the Meiyu-Baiu rainband: Environmental forcing by the westerly jet, *J. Clim.*, *23*(1), 113–134, doi:10.1175/2009JCLI3128.1.
- Sano, M., P. Tshering, J. Komori, K. Fujita, C. Xu, and T. Nakatsuka (2013), May–September precipitation in the Bhutan Himalaya since 1743 as reconstructed from tree-ring cellulose $\delta^{18}\text{O}$, *J. Geophys. Res. Atmos.*, *118*, 8399–8410, doi:10.1002/jgrd.50664.
- Saurer, M., S. Borella, and M. Leuenberger (1997a), $\delta^{18}\text{O}$ of tree rings of beech (*Fagus sylvatica*) as a record of $\delta^{18}\text{O}$ of the growing season precipitation, *Tellus B*, *49*(1), 80–92.
- Saurer, M., K. Aellen, and R. Siegwolf (1997b), Correlating $\delta^{13}\text{C}$ and $\delta^{18}\text{O}$ in cellulose of trees, *Plant Cell Environ.*, *20*(12), 1543–1550, doi:10.1046/j.1365-3040.1997.d01-53.x.
- Saurer, M., A. V. Kirydanov, A. S. Prokushkin, K. T. Rinne, and R. T. W. Siegwolf (2015), The impact of an inverse climate-isotope relationship in soil water on the oxygen-isotope composition of *Larix gmelinii* in Siberia, *New Phytol.*, *209*(3), 955–964, doi:10.1111/nph.13759.
- Schiemann, R., D. Lüthi, and C. Schär (2009), Seasonality and interannual variability of the westerly jet in the Tibetan Plateau region, *J. Clim.*, *22*(11), 2940–2957, doi:10.1175/2009JCLI2625.s1.
- Shimada, T., M. Sawada, and T. Iwasaki (2014), Indices of cool summer climate in northern Japan: Yamase indices, *J. Meteorol. Soc. Jpn*, *92*(1), 17–35, doi:10.2151/jmsj.2014-102.
- Song, X., M. M. Barbour, G. D. Farquhar, D. R. Vann, and B. R. Helliker (2013), Transpiration rate relates to within- and across-species variations in effective path length in a leaf water model of oxygen isotope enrichment, *Plant Cell Environ.*, *36*(7), 1338–1351, doi:10.1111/pce.12063.
- Sternberg, L. S. L., M. J. DeNiro, and R. A. Savidge (1986), Oxygen isotope exchange between metabolites and water during biochemical reactions leading to cellulose synthesis, *Plant Physiol.*, *82*(2), 423–427, doi:10.1104/pp.82.2.423.
- Sternberg, L. S. L. O. (2008), Oxygen stable isotope ratios of tree-ring cellulose: The next phase of understanding, *New Phytol.*, *181*(3), 553–562, doi:10.1111/j.1469-8137.2008.02661.x.
- Stott, P. A., N. P. Gillett, G. C. Hegerl, D. J. Karoly, D. A. Stone, X. Zhang, and F. Zwiers (2010), Detection and attribution of climate change: A regional perspective, *Wiley Interdiscip. Rev. Clim. Change*, *1*, 192–211, doi:10.1002/wcc.34.
- Tanaka, M. (1997), Interannual and interdecadal variations of the western North Pacific monsoon and Baiu rainfall and their relationship to the ENSO cycles, *J. Meteorol. Soc. Jpn*, *75*(6), 1109–1123.
- Tatman, C. D. (1989), *The Green Archipelago: Forestry in Preindustrial Japan*, pp. 1–336, Univ. of California Press, Berkeley.
- Treydte, K. S., G. H. Schleser, G. Helle, D. C. Frank, M. Winiger, G. H. Haug, and J. Esper (2006), The twentieth century was the wettest period in northern Pakistan over the past millennium, *Nature*, *440*(7088), 1179–1182, doi:10.1038/nature04743.
- Wang, Y. (1992), Effects of blocking anticyclones in Eurasia in the rainy season (Meiyu/Baiu season), *J. Meteorol. Soc. Jpn*, *70*(5), 929–951.
- Wigley, T., K. Briffa, and P. Jones (1984), On the average of correlated time series, with applications in dendroclimatology and hydrometeorology, *J. Clim. Appl. Meteorol.*, *23*, 201–213.

- Woodruff, S. D., et al. (2010), ICOADS release 2.5: extensions and enhancements to the surface marine meteorological archive, *Int. J. Climatol.*, *31*(7), 951–967, doi:10.1002/joc.2103.
- Xie, S.-P., K. Hu, J. Hafner, H. Tokinaga, Y. Du, G. Huang, and T. Sampe (2009), Indian Ocean capacitor effect on Indo–Western Pacific climate during the summer following El Niño, *J. Clim.*, *22*(3), 730–747, doi:10.1175/2008JCLI2544.1.
- Xie, S.-P., Y. Du, G. Huang, X.-T. Zheng, H. Tokinaga, K. Hu, and Q. Liu (2010), Decadal Shift in El Niño Influences on Indo–Western Pacific and East Asian climate in the 1970s, *J. Clim.*, *23*(12), 3352–3368, doi:10.1175/2010JCLI3429.1.
- Xu, C., M. Sano, and T. Natsuka (2011), Tree-ring cellulose $\delta^{18}\text{O}$ of *Fokienia hodginsii* in Northern Laos: A promising proxy to reconstruct ENSO?, *J. Geophys. Res.*, *116*, D24109, doi:10.1029/2011JD016694.
- Xu, C., H. Zheng, T. Nakatsuka, and M. Sano (2013), Oxygen isotope signatures preserved in tree-ring cellulose as a proxy for rainy season precipitation in southeast China, *J. Geophys. Res. Atmos.*, *118*(23), 12,805–12,815, doi:10.1002/2013JD019803.
- Xu, C., H. Zheng, T. Nakatsuka, M. Sano, Z. Li, and J. Ge (2016), Inter- and intra-annual tree-ring cellulose oxygen isotope variability in response to precipitation in southeast China, *Trees*, *30*, 785–794, doi:10.1007/s00468-015-1320-2.
- Yakir, D., and M. J. DeNiro (1990), Oxygen and hydrogen isotope fractionation during cellulose metabolism in *Lemna gibba* L., *Plant Physiol.*, *93*(1), 325–332.
- Yamanaka, T., Y. Makino, Y. Wakiyama, K. Kishi, K. Maruyama, M. Kano, W. Ma, and K. Suzuki (2015), How reliable are modeled precipitation isoscapes over a high-relief mountainous region?, *Hydrol. Res. Lett.*, *9*(4), 118–124, doi:10.3178/hrl9.118.
- Yihui, D., and J. C. L. Chan (2005), The East Asian summer monsoon: An overview, *Meteorol. Atmos. Phys.*, *89*(1–4), 117–142, doi:10.1007/s00703-005-0125-z.